*J. Fluid Mech.* (2002), *vol.* 453, *pp.* 39–55. © 2002 Cambridge University Press 
DOI: 10.1017/10.1017/S0022112001006553 Printed in the United Kingdom

# Boundary layer development on a semi-infinite suddenly heated vertical plate

By JOHN C. PATTERSON[1], TASMAN GRAHAM[2]†, WOLFGANG SCHÖPF[1]‡ AND S. W. ARMFIELD[3]

[1]School of Engineering, James Cook University, Townsville, QLD 4811 Australia

[2]Department of Environmental Engineering, University of WA, Nedlands, WA 6907 Australia

[3]Department of Mechanical and Mechatronic Engineering, University of Sydney, Sydney NSW 2006 Australia

(Received 30 March 2000 and in revised form 7 July 2001)

The flow resulting from suddenly heating a semi-infinite, vertical wall immersed in a stationary fluid has been described in the following way: at any fixed position on the plate, the flow is initially described as one-dimensional and unsteady, as though the plate is doubly infinite; at some later time, which depends on the position, a transition occurs in the flow, known as the leading-edge effect (LEE), and the flow becomes two-dimensional and steady. The transition is characterized by the presence of oscillatory behaviour in the flow parameters, and moves with a speed greater than the maximum fluid velocities present in the boundary layer. A stability analysis of the one-dimensional boundary layer flow performed by Armfield & Patterson (1992) showed that the arrival times of the LEE determined by numerical experiment were predicted well by the speed of the fastest travelling waves arising from a perturbation of the initial one-dimensional flow. In this paper, we describe an experimental investigation of the transient behaviour of the boundary layer on a suddenly heated semi-infinite plate for a range of Rayleigh and Prandtl numbers. The experimental results confirm that the arrival times of the LEE at specific locations along the plate, relatively close to the leading edge, are predicted well by the Armfield & Patterson theory. Further, the periods of the oscillations observed following the LEE are consistent with the period of the maximally amplified waves calculated from the stability result. The experiments also confirm the presence of an alternative mechanism for the transition from one-dimensional to two-dimensional flow, which occurs in advance of the arrival of the LEE at positions further from the leading edge.

## 1. Introduction

The flow induced adjacent to a vertical heated wall is one of the classical heat and mass transport problems with significance for both fundamental fluid mechanics and a wide range of engineering applications. Of particular classical interest is the case of a semi-infinite wall which is initially at the same temperature as the surrounding fluid; at some instant, the wall is suddenly heated, either by a rise in wall temperature or the imposition of a fixed heat flux.

The resulting flow has been described qualitatively in the following terms (Siegal

† Present address: Maunsell McIntyre, P.O. Box 1823, Milton, QLD 4064, Australia.
‡ Present address: Experimentalphysik V, Universitaet Bayreuth, 95440 Bayreuth, Germany.

https://doi.org/10.1017/S0022112001006553 Published online by Cambridge University Press

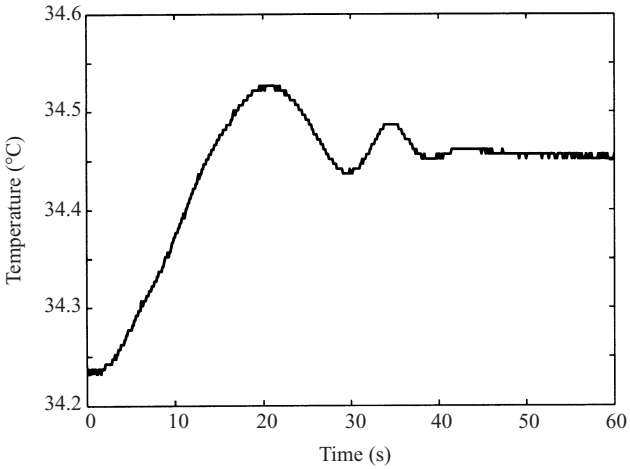



FIGURE 1. Typical temperature time series in the boundary layer, 8.75 cm downstream from the leading edge, 2.70 mm in from the wall and with an imposed temperature difference of 1.17 °C. These data were taken from experiment 22 described below.

1958). At any fixed position downstream of the end of the plate (defined as the leading edge of the plate) the flow behaves initially as though the plate were doubly infinite, and the classical unsteady one-dimensional flow and temperature fields described by Schetz & Eichorn (1962) and, in a more general context, Goldstein & Briggs (1964) are appropriate. At some later time however, depending on the distance from the leading edge, the flow becomes two-dimensional and steady, following the description by Ostrach (1964). This transition from unsteady one-dimensional flow to steady two-dimensional flow occurs over a non-zero time period, and travels downstream at some velocity which is determined by the parameters of the problem. The transition phase, referred to as the 'leading-edge effect (LEE)', is characterized by the presence of an oscillatory component, the amplitude of which is also determined by the parameters of the problem and the location, with the oscillations growing in amplitude with increasing downstream position. According to this description therefore, a time series of temperature taken at any given point in the boundary layer will initially follow the complementary error function growth given by the one-dimensional conduction solution referred to above, developing into a transition period which will include an oscillatory component, followed by an approximately constant value given by the steady-state solution of Ostrach (1964).

These three phases of the development are clearly evident in figure 1, which shows a typical temperature time series in water, taken in the boundary layer 8.75 cm downstream from the leading edge, 2.70 mm in from the wall and with an imposed temperature difference of 1.17 °C. The ambient temperature in this case was 34.24 °C.

The figure shows that in the initial part of the time series the temperature rises in a form which at least qualitatively resembles the one-dimensional temperature solution before reaching a maximum, followed by a period of oscillation decaying to an approximately steady state. The first maximum appears to represent a longer-period signal than the following oscillation and is usually referred to as an 'overshoot'. At least one period of the following oscillation is clearly present, with a period of approximately 10.4 s. By approximately 50 s, the signal is almost steady at 34.45 °C, and remains approximately constant. The full time series is not shown here; after 300 s, the temperature is steady at 34.43 °C.

https://doi.org/10.1017/S0022112001006553 Published online by Cambridge University Press

Similar figures may be drawn for other locations along the plate, at least for those close to the leading edge. Thus at each vertical location along the plate, the flow develops initially as a one-dimensional solution for the doubly infinite plate, and the presence of the upstream end is not felt until the leading-edge effect arrives. With the assumption that the effect was advected by the boundary layer flow, a propagation distance $y_p$ at time $\tau$ of the leading-edge effect was proposed by Goldstein & Briggs (1964) as

$$y_p(\tau) = \max \int_0^\tau v(x,t)\,\mathrm{d}t, \tag{1.1}$$

where $x$ is the horizontal coordinate, $v$ the vertical velocity obtained from the one-dimensional solution (given below by (4.1)), $t$ the time and the maximum is taken over $x$. Goldstein & Briggs (1964) developed results for $y_p$ for imposed flux and temperature wall conditions. On a different premise, Brown & Riley (1973) gave a slightly different estimate for the increased wall temperature case,

$$y_p(\tau) = \int_0^\tau \max[v(x,t)]\,\mathrm{d}t, \tag{1.2}$$

where again the maximum is taken over $x$, which gives a slightly higher propagation speed than (1.1). This estimate was also based on the assumption that the effect was carried by the main flow.

The early experiments to determine the properties of these flows were exclusively for suddenly imposed isoflux boundary conditions (see Gebhart & Mahajan 1982; Joshi & Gebhart 1987). The latter paper also reported the presence of a deviation from the one-dimensional solution (for the isoflux boundary condition) at all downstream locations prior to the passage of the leading-edge effect, suggesting the existence of an alternative mechanism for the transition to two-dimensional flow. This form of transition occurred for high heating rates only.

A comprehensive overview of the character of the transition to two-dimensionality based on the leading-edge effect was given in Gebhart *et al.* (1988). That review gave several possible one-dimensional solutions, and discussed the isoflux experiments which identified the passage of the leading-edge effect. The review also considered the effect of the heat capacity of the boundary itself.

More recently, in the context of a closed cavity suddenly heated and cooled isothermally from the sides, Patterson & Armfield (1990) showed that the leading-edge effect was also present on a finite vertical heated plate with horizontal boundaries, and that the description of the boundary layer development described above approximately held. A number of numerical experiments in the context of the isothermally forced cavity flow (Schladow 1990; Armfield & Patterson 1992) and the experiments of Schöpf & Patterson (1995), also for the cavity flow, reinforced this view.

One common feature of all of these investigations was that it appeared that, at a given time, the penetration distance of the leading edge effect was significantly greater than that predicted by (1.1) or (1.2). A much better prediction of the speed at which the leading edge effect travelled was given by Armfield & Patterson (1992). Their prediction was based on the speed of the fastest travelling wave of the group of waves generated on the one-dimensional boundary layer solution by the perturbation introduced at the sudden start-up of the flow. This also showed that the oscillatory behaviour that followed the transition to two-dimensional behaviour was in the same wavenumber range as the maximally amplified waves generated by the perturbation. Daniels & Patterson (1997) showed analytically that disturbances with the largest

https://doi.org/10.1017/S0022112001006553 Published online by Cambridge University Press

growth rates indeed travelled with a phase velocity greater than the maximum flow speed of the boundary layer. Still in the context of the cavity flow, experiments by Schöpf & Patterson (1995) visualized the presence of these amplifying travelling waves on the vertical boundary layers formed following sudden heating and cooling.

A recent paper (Brooker *et al.* 2000) also focused on the stability properties of the one-dimensional boundary layer generated by a suddenly imposed isothermal boundary condition. Of particular relevance to the present paper was the description of the comparison of the results of a numerical solution of the full equations of motion with the corresponding results from a single experiment from the series reported below, although there was only a brief description of the experimental procedures themselves. Only one comparison was described.

This single parameter group of results was shown to compare well with the numerical solution, but there was no discussion of the speed of travel or other properties of the leading-edge effect. Brooker *et al.* (2000) did however discuss the second form of transition to two-dimensionality mentioned above, although they did not specifically identify it as a form of transition. In their paper, a numerical simulation of the side-heated cavity start-up flow was subjected to random perturbations in temperature along the length of the vertical wall; by adjusting the amplitude of the perturbations, simulated temperature time series at three locations in the downstream half of the wall were shown to closely match those observed at corresponding locations in the experiments, chosen from those data which showed a transition well ahead of the arrival of the leading-edge effect. This result was identified as a convective instability in the boundary layer, and it was argued that in the experiments, this particular instability was triggered by the vibrations necessarily present on the experimental rig. The paper did not contain a discussion of this feature in the context of a transition to two-dimensionality.

All of these recent papers relating to the isothermal vertical plate were (other than Daniels & Patterson 1997) in the context of the cavity flow, in which fixed horizontal boundaries were present at either end of the finite vertical plate. In the present paper, an experimental investigation of an approximation to a vertical semi-infinite plate, suddenly heated to a temperature above ambient and maintained at that temperature, is described. The results confirm that the leading edge effect travels at a speed greater than that implied by (1.1) and (1.2). The model suggested by Armfield & Patterson (1992) is investigated by the calculation of the maximum wave speeds on the one-dimensional boundary layer, and shown to be in much better agreement with the experimental results than (1.1) or (1.2). The periods of the oscillations observed following the leading-edge effect are shown to be consistent with the periods of the maximally amplified travelling waves predicted by the stability analysis. These observations lend strong support to the Armfield & Patterson (1992) model for the leading-edge effect transition mechanism. The experiments also confirm the presence of the alternative mechanism of transition to a two-dimensional flow, but a detailed discussion of that mechanism is outside the scope of this paper.

Finally, we note that, although these experiments were briefly mentioned in Brooker *et al.* (2000), the description there was brief and referred only to a single experimental set which identified the existence of the convective instability present at the downstream end of the one-dimensional boundary layer. That paper did not address any of the issues relating to the properties of the leading-edge effect, and in particular did not provide any information with respect to the speed of travel, or of the properties of the oscillatory behaviour following the leading-edge effect.

https://doi.org/10.1017/S0022112001006553 Published online by Cambridge University Press

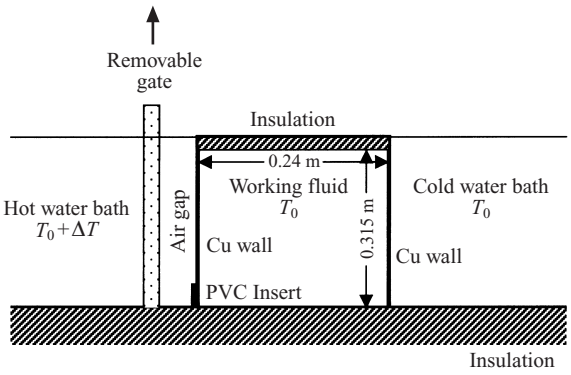



FIGURE 2. Experimental setup.

## 2. Experimental methods

The experimental rig for investigating the transient response of the boundary layer on the semi-infinite plate following a sudden increase in the plate temperature was based on that used in the side heated and cooled cavity experiments (Patterson & Armfield 1990). In this rig, the semi-infinite plate is modelled by a vertical $24 \times 50$ cm, 1.15 mm thick copper plate. The lower end of the plate is smoothly joined to a $7.5 \times 50$ cm sheet of 1.5 cm thick PVC. This composite plate forms one boundary to the working fluid container, which is $24 \times 31.5 \times 50$ cm. The opposing boundary is also of copper, while the floor, roof and two endwalls are constructed from 1.9 cm thick Perspex, and lined with polystyrene foam insulation. The opposing wall is maintained at the initial temperature $T_0$ of the working fluid by a large water bath. The semi-infinite plate is separated from a large hot water bath, maintained at $T_0 + \Delta T$ by a combination of heating and cooling elements, by a 3 cm air gap, restrained by a pneumatically operated gate. The air gap is maintained at $T_0$ by a heat exchanger embedded in the gate. By maintaining the air gap at the initial temperature, heat transfer to the copper wall prior to the start of the experiment is minimized. A schematic of the rig (not to scale) is shown in figure 2.

The experiment is initiated by rapidly raising the gate, allowing the heated water to flood against the copper wall, with full thermal contact being achieved in a fraction of a second. The thermal response time of the copper plate is $O(10^{-2})$ s, very much shorter than any time scale associated with the setting up of the boundary layer (Patterson & Imberger 1980). This method of rapid heating has been successfully used in a series of differentially heated cavity experiments, in which the opposing wall is cooled at the same time and in the same way (Patterson & Armfield 1990; Jeeveraj & Patterson 1992; Schöpf & Patterson 1995, 1996).

The configuration of the heated wall is not precisely that of a true semi-infinite plate which has a free end suspended in the ambient fluid. The flow and temperature fields around a freely suspended plate could be expected to be symmetric about the line of the plate, including the region beyond the extent of the plate, that is, upstream of the leading edge. Our model has replaced the space beyond the leading edge with a PVC wall. The wall is insulated, so the symmetry of the temperature field is preserved. Further, a zero transverse velocity would be expected on the line of symmetry below the plate, which again is preserved by the PVC wall. The vertical velocity on the line of symmetry is forced by our model to be zero, which may not be the case in a freely suspended plate. We note however that the numerically evaluated vertical velocities

https://doi.org/10.1017/S0022112001006553 Published online by Cambridge University Press

below the plate are extremely small (Wright & Gebhart 1994) and this error is thought to be small, and will not influence the subsequent development of the boundary layer.

The constraints of the working fluid space also affect the downstream end of the boundary layer. Here, a solid horizontal wall forces the boundary layer to exit into the working space as a horizontal intrusion similar to that observed in the cavity flow. Ultimately this intrusion will impact on the opposing wall and a wave will be reflected back along the intrusion interface. The intersection of this reflected wave with the downstream end of the boundary layer will significantly affect the layer properties. However, the time scale for this is well beyond the time at which the leading-edge effect has passed through the full extent of the layer, which is essentially in steady state when this interaction occurs. Likewise, the presence of the downstream corner will only affect the region immediately adjacent to the corner.

Temperature measurements in the boundary layer were made with Thermometric FP07 fast response thermistors. The body of these thermistors has a maximum diameter of 2.2 mm, though the thermistor itself is contained in a small thin glass bead of maximum diameter less than 0.2 mm. The thermistors have a time constant in water of 7 ms. The thermistor bodies were mounted in insulated 2.5 mm tubes inserted at an angle through the lid of the cavity and of sufficient length to enable placement along the vertical wall. The output from the thermistors was preamplified before being sampled by a 12 bit A-D board at 10 Hz. After calibration, the overall accuracy of the measurement was 0.04 °C. These thermistors were placed at various distances downstream from the leading edge, ranging from 3.45 to 21 cm, depending on the particular sequence of experiments, and at distances out from the plate ranging from 1.5 to 3.5 mm. Because of the high horizontal temperature gradient expected in the boundary layer, the lateral positioning will strongly affect the temperature measured. The longitudinal gradients are much less, and positioning is less crucial. In both cases, the positioning was accurate to within 0.5 mm. A fitting procedure gave a more accurate lateral position, as discussed below. Additional thermistors were placed in the interior of the working fluid to give the ambient temperature, in the hot water bath, and on the interior side of the copper plate to give accurate measurements of the wall temperature. The thermistors were staggered across the width of the plate to prevent any downstream influence.

All of the experiments were performed with water as the working fluid. The resulting flows are characterized by the Prandtl number $Pr$ and the Rayleigh number $Ra$, where

$$Pr = \frac{\nu}{\kappa}, \tag{2.1}$$

$$Ra = \frac{g\beta\Delta T h^3}{\nu\kappa}, \tag{2.2}$$

and $\nu$ and $\kappa$ are the kinematic viscosity and thermal diffusivity of water respectively, $\beta$ the coefficient of thermal expansion, $h$ the height of the plate and $\Delta T$ the applied temperature difference. Although in the truly semi-infinite plate there is no natural physical length scale, using the plate height (24 cm) in the definition of $Ra$ provides a useful means of classifying the various experiments.

The third phase of the typical temperature time series in figure 1 shows that the boundary layer is essentially steady, and may be assumed to be described by the solution given by Ostrach (1964) for the given parameter values. Although not available in closed form, this solution may be readily computed for given $x$ and $y$ locations and $Ra$ and $Pr$ values. In particular, for each time series, for the given $y$

https://doi.org/10.1017/S0022112001006553 Published online by Cambridge University Press

| Expt | $T_0$ (°C) | $Ra$ | $Pr$ | $\Delta T$ (°C) | $\kappa$ (m$^2$ s$^{-1}$) | $\nu$ (m$^2$ s$^{-1}$) | $\beta$ (°C$^{-1}$) |
|---|---|---|---|---|---|---|---|
| 18 | 27.89 | $1.89 \times 10^9$ | 5.42 | 5.33 | $1.46 \times 10^{-7}$ | $7.94 \times 10^{-7}$ | $3.04 \times 10^{-4}$ |
| 19 | 28.88 | $1.68 \times 10^9$ | 5.34 | 4.60 | $1.47 \times 10^{-7}$ | $7.84 \times 10^{-7}$ | $3.09 \times 10^{-4}$ |
| 20 | 29.96 | $1.33 \times 10^9$ | 5.27 | 3.57 | $1.47 \times 10^{-7}$ | $7.75 \times 10^{-7}$ | $3.14 \times 10^{-4}$ |
| 21 | 31.81 | $1.47 \times 10^9$ | 5.04 | 3.65 | $1.48 \times 10^{-7}$ | $7.46 \times 10^{-7}$ | $3.29 \times 10^{-4}$ |
| 22 | 34.25 | $4.94 \times 10^8$ | 4.89 | 1.17 | $1.49 \times 10^{-7}$ | $7.28 \times 10^{-7}$ | $3.39 \times 10^{-4}$ |
| 23 | 20.73 | $1.62 \times 10^9$ | 6.40 | 6.34 | $1.44 \times 10^{-7}$ | $9.18 \times 10^{-7}$ | $2.49 \times 10^{-4}$ |
| 24 | 20.84 | $2.40 \times 10^9$ | 6.18 | 8.66 | $1.44 \times 10^{-7}$ | $8.90 \times 10^{-7}$ | $2.62 \times 10^{-4}$ |
| 25 | 21.43 | $2.05 \times 10^9$ | 6.19 | 7.43 | $1.44 \times 10^{-7}$ | $8.91 \times 10^{-7}$ | $2.61 \times 10^{-4}$ |
| 26 | 21.81 | $1.59 \times 10^9$ | 6.25 | 5.89 | $1.44 \times 10^{-7}$ | $9.00 \times 10^{-7}$ | $2.57 \times 10^{-4}$ |
| 27 | 21.71 | $1.62 \times 10^9$ | 6.26 | 6.00 | $1.44 \times 10^{-7}$ | $9.00 \times 10^{-7}$ | $2.57 \times 10^{-4}$ |
| 28 | 21.02 | $1.10 \times 10^9$ | 6.51 | 4.45 | $1.43 \times 10^{-7}$ | $9.33 \times 10^{-7}$ | $2.42 \times 10^{-4}$ |
| 29 | 21.10 | $8.22 \times 10^8$ | 6.59 | 3.43 | $1.43 \times 10^{-7}$ | $9.42 \times 10^{-7}$ | $2.38 \times 10^{-4}$ |
| 30 | 21.06 | $6.03 \times 10^8$ | 6.67 | 2.59 | $1.43 \times 10^{-7}$ | $9.52 \times 10^{-7}$ | $2.33 \times 10^{-4}$ |
| 31 | 21.05 | $3.33 \times 10^8$ | 6.76 | 1.48 | $1.43 \times 10^{-7}$ | $9.65 \times 10^{-7}$ | $2.28 \times 10^{-4}$ |

TABLE 1. Parameter values for the 14 experiments considered.

location, a horizontal position may be determined so that the Ostrach solution value of temperature, for the given applied temperature difference, matches the observed value. This may then be taken as an estimate of the actual $x$ position of the thermistor, and should be close to the measured position. This procedure was carried out for all experimental time series. The largest errors occurred for the thermistors closest to the plate; other than for these, the estimated and measured locations were within the measurement accuracy of 0.5 mm. The thermistors measured as being located within 1.5 mm of the wall gave errors of less than 1 mm.

## 3. Results

The results from 14 separate experiments, numbered from 18 to 31, are reported here, with $\Delta T$ ranging from 1.17 °C to 8.66 °C, and the ambient temperature $T_0$ ranging from 20.73 °C to 34.25 °C. The experiments fell broadly into two groups; experiments 18–22 in which $T_0$ was in the range 27.89 °C to 34.25 °C; and experiments 23–31 in which $T_0$ was in the range 20.73 °C to 21.81 °C. The various combinations and derived quantities are shown in table 1. Note that the derived quantities are calculated at the average boundary layer temperature $T_0 + \Delta T/2$. Shown in table 2 are the locations of the thermistors in each sequence of experiments. The $x$ values are those determined by the fitting procedure.

Each experiment gives rise to a time series of temperature at each of the thermistor locations. A typical set, from experiment 21 in which four thermistors were located in the boundary layer, is shown in figure 3. Here $\Delta T = 3.65$ °C, and the corresponding values of $Ra$ and $Pr$ are $1.47 \times 10^9$ and 5.04 respectively, and only the first 70 s is shown. The $y$ locations (in cm downstream from the leading edge) of the four thermistors are marked on each of the time series traces.

Consider first the two traces at $y = 3.45$ cm and $y = 8.75$ cm. Both show an initial behaviour similar to the expected one-dimensional solution growth, before deviating into a temperature maximum, followed by a decaying oscillatory period. The signal closest to the leading edge shows a rise to a peak, usually referred to as the overshoot, followed by an oscillation in which a single period can be clearly identified. The signal at $y = 8.75$ cm again shows the overshoot, followed by several periods with

https://doi.org/10.1017/S0022112001006553 Published online by Cambridge University Press

| Expt | $y$ (cm) | $x$ (mm) |
|---|---|---|
| 18–22 | 3.45 | 2.52 |
| | 8.75 | 2.70 |
| | 16.65 | 2.27 |
| | 20.60 | 2.51 |
| 23–31 | 8.85 | 2.72 |
| | 11.75 | 1.80 |
| | 12.55 | 3.66 |
| | 13.95 | 3.05 |
| | 16.65 | 3.19 |
| | 20.65 | 2.72 |

TABLE 2. Thermistor locations for the 14 experiments considered.

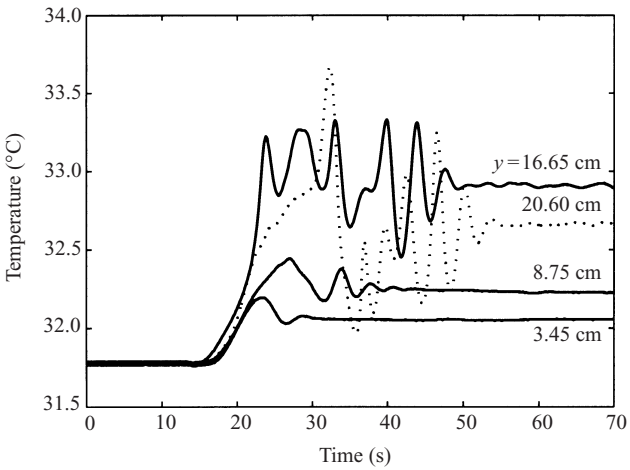



FIGURE 3. Temperature time series from experiment 21.

an amplitude greater than the lower signal. This is consistent with the model of a travelling transition region which is characterized by an oscillatory behaviour; the increasing amplitude indicates that the boundary layer is unstable to the wavenumber of these signals. This aspect will be discussed below; it suffices to note at this point that these signals are of a wavenumber consistent with that obtained by a stability analysis of the one-dimensional boundary layer. The approximately steady-state temperatures reached are consistent with the thickening boundary layer. These thermistors are located at 2.52 and 2.70 mm from the wall respectively and although the upper thermistor is marginally further removed from the wall, suggesting a lower temperature, this is evidently approximately compensated for by its position further downstream in a wider boundary layer.

The third thermistor (upper solid line) is located 16.65 cm from the leading edge, and 2.27 mm from the wall. The steady-state temperature is significantly higher than the previous two signals, again consistent with the increased distance up the plate and its relative proximity to the plate. The early time behaviour of this signal however is not precisely what was expected. The deviation from the one-dimensional solution appears sooner than the simple growth model predicts, and there appear to be at least two wavenumbers present. The signal from the thermistor placed at 20.60 cm

https://doi.org/10.1017/S0022112001006553 Published online by Cambridge University Press

(broken line) has a similar behaviour during early time; further, the steady state is at a temperature lower than that of the thermistor below. This thermistor is placed at a distance 2.51 mm from the wall. Consequently the steady-state temperature is lower than that of the third thermistor, which is closer to the heated wall.

The complex initial behaviour of the signals from the third and fourth thermistors is evidently the result of an instability forming everywhere on the one-dimensional boundary layer before the arrival of the leading-edge effect. As discussed earlier, Brooker *et al.* (2000) have shown that this effect may be accurately predicted numerically by imposing a random perturbation to the temperature boundary condition on the wall in the numerical solution of the cavity formulation of this problem. Evidently the one-dimensional boundary layer becomes unstable as time increases, and the perturbations introduced along the wall by the experimental conditions are sufficient to trigger a convective instability on the boundary layer downstream of the travelling transition region, that is before the transition region arrives. The consequence of this is the appearance of oscillatory signals before the arrival of the leading-edge effect, and the expected complementary error-function-like rise followed by the oscillatory period is strongly modified by the presence of these additional oscillations. This is a clear demonstration that an alternative mechanism for the transition to two-dimensionality exists, consistent with the observation reported in Joshi & Gebhart (1987). The evidence of the presence of this mechanism in almost all of the downstream thermistor time series means that, in fact, the passage of the leading edge effect is the transition mechanism in the upstream part of the boundary layer only. This limits the estimate of the speed of the leading-edge effect to the first thermistor in experiments 23–31, and the first two thermistors in experiments 18–22. The alternative form of transition to two-dimensionality is discussed briefly below.

## 4. Leading-edge-effect propagation

The estimates of the arrival time of the leading-edge effect given by (1.1) and (1.2) are based on the one-dimensional solution of Schetz & Eichorn (1962) for the flow adjacent to a suddenly heated vertical plate. The vertical velocity $v_{GB}(x,t)$ and the temperature $T_{GB}(x,t)$ at lateral position $x$ and time $t$ are given by, for $Pr > 1$,

$$v_{GB}(x,t) = \frac{4g\beta\Delta T t}{1-Pr}\left[i^2\,\mathrm{erfc}\left(\frac{x}{2\sqrt{\kappa t}}\right) - i^2\,\mathrm{erfc}\left(\frac{x}{2\sqrt{\nu t}}\right)\right], \tag{4.1}$$

and

$$T_{GB}(x,t) = T_0 + \Delta T\,\mathrm{erfc}\left(\frac{x}{2\sqrt{\kappa t}}\right), \tag{4.2}$$

where $T_0$ is the initial temperature, $i^2\mathrm{erfc}(z)$ is the second integral of the complementary error function $\mathrm{erfc}(z)$ with argument $z$ (see e.g. Abramowitz & Stegun 1965). The other variables are given above. The special case for $Pr = 1$ is given in Schetz & Eichorn (1962), but is not relevant to the water experiments described here.

According to the simple conceptual model of the way in which the boundary layer develops, the temperature distribution given by (4.2) should describe the early part of the temperature time series at any location on the boundary layer. The further downstream the location is, the longer the description should hold, subject of course to the presence of the secondary instability referred to above.

Figure 4 shows the single thermistor time series from figure 1 (taken from experiment 22, and located 8.75 cm from the leading edge and 2.70 mm away from the wall),

https://doi.org/10.1017/S0022112001006553 Published online by Cambridge University Press

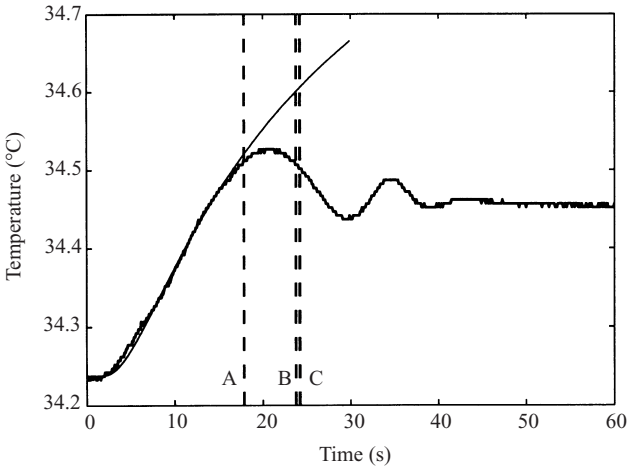



FIGURE 4. A single thermistor time series from experiment 22, showing $t_{CR}$, $t_{BR}$ (B), $t_{GB}$ (C) and the one-dimensional temperature solution for the position of the thermistor.

together with the one-dimensional solution, given by (4.2), for the parameters for this particular time series. As expected, the one-dimensional solution closely matches the early part of the time series, but deviates from it at approximately $t = 15\,\mathrm{s}$. The deviation of the signal from the one-dimensional solution marks the arrival of two-dimensional information, that is the arrival of the leading-edge effect.

The first of the two estimates for the arrival of the leading edge effect requires integration of $v_{GB}(x,t)$ before the maximization is carried out. This yields the following expression for the penetration distance $y_p(\tau)$:

$$y_p(x,\tau) = \frac{4g\beta\Delta T}{1-Pr}(Y_{\alpha_\kappa} - Y_{\alpha_\nu}), \tag{4.3}$$

where

$$Y_\alpha = \left(\frac{\alpha^2\tau}{2} + \frac{\tau^2}{8} + \frac{\alpha^4}{6}\right)\mathrm{erfc}\left(\frac{\alpha}{\sqrt{\tau}}\right) - \left(\frac{\alpha^3\sqrt{\tau}}{6} + \frac{5\alpha\tau^{3/2}}{12}\right)\frac{\exp(-\alpha^2/\tau)}{\sqrt{\pi}}, \tag{4.4}$$

with

$$\alpha_\kappa = \frac{x}{2\sqrt{\kappa}} \tag{4.5}$$

and

$$\alpha_\nu = \frac{x}{2\sqrt{\nu}}. \tag{4.6}$$

For any given $\tau$, the maximum value of $y_p(x,\tau)$ over $x$ gives the penetration distance $y_{GB}(\tau)$. Interpolation then yields the time $t_{GB}$ to achieve a particular penetration distance.

On the other hand (1.2) can be simplified since $v_{GB}(x,t)$ can be written as

$$v_{GB}(x,t) = \frac{4g\beta\Delta T t}{Pr-1}U(\eta), \tag{4.7}$$

where

$$U(\eta) = i^2\,\mathrm{erfc}(\eta/\sqrt{Pr}) - i^2\,\mathrm{erfc}(\eta), \tag{4.8}$$

https://doi.org/10.1017/S0022112001006553 Published online by Cambridge University Press

| Expt | $y_t$ (cm) | $t_{BR}$ (s) | $t_{GB}$ (s) | $t_{act}$ (s) | $\frac{t_{BR}}{t_{act}}$ | $\frac{t_{GB}}{t_{act}}$ | $t_{CR}$ (s) | $\frac{t_{CR}}{t_{act}}$ |
|---|---|---|---|---|---|---|---|---|
| 18 | 3.45 | 7.61 | 7.75 | 5.42 | 1.40 | 1.43 | 5.73 | 1.06 |
| 18 | 8.75 | 12.14 | 12.36 | 7.19 | 1.69 | 1.75 | 9.12 | 1.27 |
| 19 | 3.45 | 8.10 | 8.25 | 6.01 | 1.35 | 1.37 | 6.05 | 1.01 |
| 19 | 8.75 | 12.90 | 13.15 | 10.25 | 1.26 | 1.31 | 9.65 | 0.94 |
| 20 | 3.45 | 9.08 | 9.25 | 4.30 | 2.11 | 2.16 | 6.83 | 1.59 |
| 20 | 8.75 | 14.46 | 14.74 | 6.43 | 2.25 | 2.37 | 10.87 | 1.69 |
| 21 | 3.45 | 8.63 | 8.79 | 7.48 | 1.15 | 1.18 | 6.53 | 0.87 |
| 21 | 8.75 | 13.75 | 14.02 | 9.56 | 1.44 | 1.50 | 10.39 | 1.09 |
| 22 | 3.45 | 14.91 | 15.20 | 11.12 | 1.34 | 1.71 | 11.20 | 1.01 |
| 22 | 8.75 | 23.75 | 24.21 | 15.36 | 1.55 | 2.10 | 17.84 | 1.16 |
| 23 | 8.85 | 13.09 | 13.34 | 9.80 | 1.34 | 1.36 | 9.77 | 1.00 |
| 24 | 8.85 | 10.79 | 10.99 | 6.14 | 1.76 | 1.79 | 7.99 | 1.30 |
| 25 | 8.85 | 11.67 | 11.89 | 7.81 | 1.49 | 1.52 | 8.64 | 1.11 |
| 26 | 8.85 | 13.26 | 13.50 | 9.37 | 1.42 | 1.44 | 9.83 | 1.05 |
| 27 | 8.85 | 13.14 | 13.80 | 9.02 | 1.46 | 1.48 | 9.74 | 1.08 |
| 28 | 8.85 | 15.88 | 16.30 | 10.37 | 1.53 | 1.56 | 11.75 | 1.13 |
| 29 | 8.85 | 18.39 | 18.94 | 10.63 | 1.73 | 1.76 | 13.71 | 1.29 |
| 30 | 8.85 | 21.48 | 21.89 | 13.16 | 1.63 | 1.66 | 16.07 | 1.22 |
| 31 | 8.85 | 28.82 | 29.37 | 20.56 | 1.40 | 1.43 | 21.61 | 1.05 |

TABLE 3. Tabulated values for all of the estimates of arrival time for all experiments.

with

$$\eta = \frac{x}{2\sqrt{\kappa t}}, \tag{4.9}$$

and therefore

$$y_p = \frac{4g\beta\Delta T}{Pr - 1} \max(U(\eta)) \frac{t^2}{2}. \tag{4.10}$$

In (4.10), the maximum is taken over $\eta$. Because of the similarity properties of (4.8), the maximum of $U(\eta)$ is a function of $Pr$ only, and (4.10) may be inverted to obtain the time $t_{BR}$ required to reach a particular location.

For the experiment shown in figure 4, this procedure gives $t_{BR} = 23.75$ s and $t_{GB} = 24.21$ s. These times are shown on the figure as the vertical lines marked B and C respectively. The meaning of the vertical line marked A will be discussed below.

While the procedure for determination of the time at which the time series deviates from the one-dimensional solution is yet to be discussed, it is clear that the predictions based on (1.1) and (1.2) yield an arrival time well in excess of that observed. These signals are clearly travelling at a velocity much greater than that predicted by either of these models. This result is consistent across all of the data collected in this experimental series, and is also consistent with the numerical results of Schladow (1990), Armfield & Patterson (1992), Brooker, Patterson & Armfield (1997) and the cavity experiments of Schöpf & Patterson (1995).

Table 3 gives the values of $t_{BR}$ and $t_{GB}$ for each of the time series which were not affected by the additional instability mentioned above. This restricted application to a total of 19 time series. Also in the table are the corresponding thermistor locations $y_t$. The experimental parameters for each time series are given in table 1. The variables $t_{act}$ and $t_{CR}$ will be discussed below.

The estimation of the actual departure time from one-dimensionality is a somewhat subjective process. All of the parameters of the one-dimensional solution are known:

https://doi.org/10.1017/S0022112001006553 Published online by Cambridge University Press

the temperature difference, the distance from the wall and the thermal diffusivity. In principle therefore, the one-dimensional solution simply overlays the observed temperatures, and the departure from the one-dimensional solution is simply read off according to a specified criterion for a difference between the two results. However, the temperature data are carrying some noise, there is a small ambiguity with respect to the actual starting time of the experiment, and the size of the difference criterion affects the timing of the departure.

The departure times were estimated by comparing the appropriate one-dimensional solution to the data. To confirm the timing of the start of the experiment, a least-squares fitting procedure was used to provide the best fit of the one-dimensional solution to the early part of the time series. This occasionally resulted in a small correction to the recorded start time. The time of departure from the one-dimensional solution was identified by noting the time at which the temperature difference between the two exceeded 1% of the actual value at that time. A visual check then confirmed that this was not the result of a local fluctuation due to noise and that indeed the one-dimensional solution was subsequently always greater than the recorded data. Even so, there is still some ambiguity with respect to fluctuations on the time scale of the measurement. Nevertheless, by applying this process in a consistent way, an estimate of the departure times in each case may be obtained. The times estimated for all of the experimental time series are given in table 3, as $t_{act}$.

The ratios $t_{BR}/t_{act}$ and $t_{GB}/t_{act}$ are given in table 3, and it is clear that the times $t_{BR}$ and $t_{GB}$ significantly overestimate the travel time, and in some cases are more than double the observed times.

The model proposed in Armfield & Patterson (1992) was based on the principle that the fastest travelling wave from the perturbation introduced at the leading edge by the start-up was responsible for triggering the transition to the Ostrach solution, and therefore was a measure of the arrival of the leading-edge effect. Daniels & Patterson (1997) showed that these waves always travelled at a velocity higher than the fastest advective velocity in the boundary layer, which implied that the leading-edge signal would arrive sooner than predicted by boundary layer based models.

The penetration distance $y_p(\tau)$ of the leading-edge effect at time $\tau$, following the Armfield & Patterson (1992) model, is given by

$$y_p(\tau) = \int_0^\tau c_{rmax}(t)\mathrm{d}t, \tag{4.11}$$

where $c_{rmax}$ is the maximum phase velocity at time $t$. To evaluate these integrals for the parameters given, the stability properties of the one-dimensional solutions in each case must first be determined. The formulation and solution of the linear stability analysis has been previously addressed (see e.g. Armfield & Patterson 1992; Daniels & Patterson 1997) and only a brief description is given here.

The one-dimensional solutions given by (4.1) and (4.2) are referred to as the base flow. To determine the stability properties of the base flow, it is modified by a small perturbation of the form

$$\Psi = \psi_B + \epsilon \mathrm{Re}\left[\psi(x)\mathrm{e}^{\mathrm{i}\alpha(y-c\tilde{t})}\right] \tag{4.12}$$

and

$$\Theta = T_B + \epsilon \mathrm{Re}\left[\theta(x)\mathrm{e}^{\mathrm{i}\alpha(y-c\tilde{t})}\right], \tag{4.13}$$

where $\epsilon$ is a small parameter; Re signifies the real part of the following expression; $\Psi$

https://doi.org/10.1017/S0022112001006553 Published online by Cambridge University Press

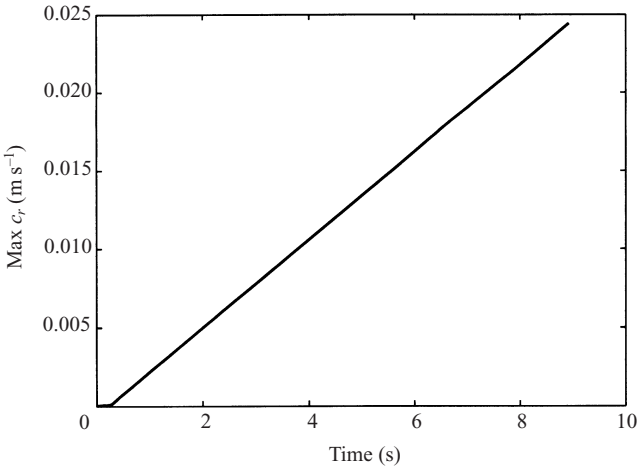



FIGURE 5. Maximum phase velocity as a function of time for experiment 31.

and $\psi$ are total and perturbation stream functions respectively, defined in the usual way; $\Theta$ and $\theta$ are total and perturbation temperatures respectively; and the subscript $B$ refers to the base flow values. Since travelling waves are sought, the wavenumber $\alpha$ is real, and $c$ is complex with real part $c_r$ and imaginary part $c_i$; $c_r$ is the wave phase speed, and $\alpha c_i$ is the amplification. Here $\tilde{t}$ is the time associated with the waves; $t$ associated with the base flow is only a parameter in the following stability analysis. This is consistent with assuming that any variations with respect to the waves are on a much faster time scale than the variations associated with the growth of the base flow (Daniels & Patterson 1997). In other words, the stability calculations are carried out at a particular time as though the base flow velocity and temperature fields were fixed at that time.

When $\Psi$ and $\Theta$ are inserted in the equations of motion, the base flow terms cancel, and the result linearized with respect to $\epsilon$, a sixth-order ordinary differential equation system for the eigenfunctions $\psi$ and $\theta$, with eigenvalues $\alpha$, $c_r$ and $c_i$, is obtained. The solution of these equations has been described in Armfield & Patterson (1992) and Daniels & Patterson (1997) and will not be discussed further here.

To evaluate the time taken for the leading-edge effect to reach a given position following this model, the maximum wave speed is required as a function of time. Thus a large number of evaluations of the wave speed spectra are required to allow an integration over time of the maximum wave speed. Again, the details of these calculations are omitted here. It is worth noting the following features however: first, at large times, the wave speed spectrum with respect to wavenumber is highly peaked, with a clear maximum; second, at large times, the maximum wave speed is at a wavenumber which is not amplified, although a significant part of the spectrum is amplified; third, as time decreases, the maximum is less well defined with a much flatter distribution; fourth, the eigenvalues become increasingly difficult to find as time decreases, which may be related to the observation that the amplified part of the spectrum is increasingly difficult to locate; and finally, apart from the time near zero, the maximum wave velocity is a evidently a linear function of time.

A typical result is shown in figure 5. In this case the result is for experiment 31, for which $Pr = 6.76$ and $\Delta T = 1.48\,^{\circ}\mathrm{C}$. The figure shows the maximum wave speed $c_r$ as a function of time $t$. Solutions at $t < 0.29$ s could not be found, but for $t > 0.29$ s, the

https://doi.org/10.1017/S0022112001006553 Published online by Cambridge University Press

dependence of $c_r$ on time is linear, with a slope of $0.379 \times 10^{-3}\,\mathrm{m\,s^{-2}}$. At $t = 0.29\,\mathrm{s}$, the velocity is $1.5 \times 10^{-4}\,\mathrm{m\,s^{-1}}$. A good approximation to this dependence on time is to assume that the velocity is zero for $t < 0.29\,\mathrm{s}$, corresponding to the intercept of the extrapolated linear function. This yields a simple inversion to calculate the time taken to reach a given $y$ location.

For the case shown in figure 4, the calculated time to reach the thermistor location at 8.75 cm is 17.84 s. This is shown on figure 4 as the vertical broken line marked A. Qualitatively at least, this estimate is a very good indicator of the time at which the response deviates from the one-dimensional solution. Figures similar to figure 4 could be drawn for each of the time series at the thermistor locations mentioned with a similar qualitative agreement; these are not included here for brevity.

The times based on the integration of the maximum wave speed have been calculated for the 19 time series suitable for comparison. The times have been entered in table 3 as $t_{CR}$. The ratio $t_{CR}/t_{act}$ has also been entered in table 3. The implications of these results are discussed in § 6.

## 5. Wave periods

The other aspect of the model suggested is that the group of waves following the transition are visible primarily as the most amplified wave in the amplified part of the spectrum at the time of observation. The time series gathered here do not contain a sufficient number of wavelengths to allow a Fourier analysis to determine the periods observed, and estimates of periods are simply peak to peak observations for those few cycles present. Consequently, these observations are somewhat qualitative. Nonetheless, it is instructive to compare these observations with those predicted by the stability analysis for the maximally amplified part of the spectrum for the times at which the waves are observed in the experiments.

Table 4 shows the observed $T_{obs}$ and predicted $T_{pred}$ wave periods for the experiments and thermistors indicated. This is only a small subset of all the time series, restricted because either there were insufficient wavelengths to make even a cursory estimate or because those wavelengths present were greatly influenced by the presence of the pre-leading-edge effect instability along the full length of the boundary layer.

## 6. Discussion

Table 3 clearly shows that $t_{CR}$ is a much better estimator for $t_{act}$ than either of $t_{BR}$ or $t_{GB}$ which both overestimate the time of arrival of the leading-edge effect. However, $t_{CR}$ is, on average, 15% greater than $t_{act}$.

The quality of $t_{CR}$ as an estimate for $t_{act}$ is shown in figure 6, which shows as solid circles the data pairs $t_{CR}$ and $t_{act}$ for the time series in table 3. Linear regression gives a slope of 1.01, very close to the expected value of 1. The $R^2$ value for the regression is 0.88. This regression line has a non-zero intercept; this is to be expected following the comments regarding calculating $t_{CR}$ at small time values.

The comparisons of the observed wave periods and those predicted by the stability analysis in table 4 are, with only a few exceptions, all within 10%. This observation needs to be tempered by the relative inaccuracy of the observations, and these figures are indicative only.

It is also of interest to consider the time of arrival of the leading-edge effect in the context of the time scale for the arrival of the travelling waves. It may be shown by approximating the stability equations that the velocity scale for the travelling wave

https://doi.org/10.1017/S0022112001006553 Published online by Cambridge University Press

| Expt | $y_t$ (cm) | time (s) | $T_{obs}$ (s) | $T_{pred}$ (s) | $\frac{T_{obs}}{T_{pred}}$ |
|---|---|---|---|---|---|
| 18 | 3.45 | 14.0 | 3.7 | 3.76 | 1.0 |
| 19 | 3.45 | 10.3 | 4.8 | 3.92 | 1.2 |
| 19 | 8.75 | 14.9 | 4.1 | 4.08 | 1.0 |
| 20 | 3.45 | 11.6 | 3.3 | 4.58 | 0.7 |
| 20 | 8.75 | 16.7 | 3.9 | 4.75 | 0.8 |
| 21 | 3.45 | 12.4 | 4.2 | 4.42 | 1.0 |
| 22 | 3.45 | 22.3 | 9.8 | 9.06 | 1.1 |
| 22 | 8.75 | 30.5 | 9.2 | 9.37 | 1.0 |
| 23 | 8.85 | 16.4 | 4.2 | 3.94 | 1.1 |
| 24 | 8.85 | 13.8 | 3.0 | 3.12 | 1.0 |
| 25 | 8.85 | 14.4 | 3.3 | 3.42 | 1.0 |
| 26 | 8.85 | 16.5 | 4.1 | 4.02 | 1.0 |
| 27 | 8.85 | 16.1 | 4.1 | 4.14 | 1.0 |
| 28 | 8.85 | 19.4 | 5.2 | 5.05 | 1.0 |
| 29 | 8.85 | 21.8 | 6.1 | 6.04 | 1.0 |
| 30 | 8.85 | 25.7 | 7.5 | 7.31 | 1.0 |
| 31 | 8.85 | 35.1 | 11.5 | 10.6 | 1.1 |

TABLE 4. Tabulated values of the predicted wave period ($T_{pred}$) and observed period ($T_{obs}$) for those experiments where a comparison is possible.

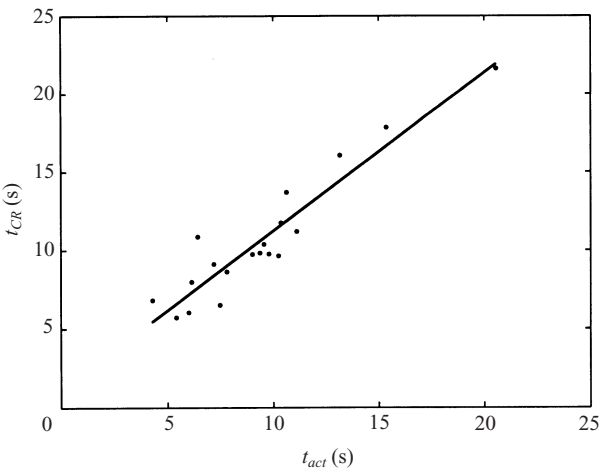



FIGURE 6. The value of the predicted arrival time of the LEE ($t_{CR}$) plotted against the observed time of arrival ($t_{act}$), from table 3.

velocity is given by, for $Pr > 1$,

$$\hat{v} \sim v_{adv}\sqrt{Pr}, \tag{6.1}$$

where $v_{adv}$ is the velocity scale of the vertical boundary layer velocity given by, from Patterson & Imberger (1990) or more directly from (4.1),

$$v_{adv} \sim \frac{g\beta\Delta T}{Pr}t, \tag{6.2}$$

https://doi.org/10.1017/S0022112001006553 Published online by Cambridge University Press

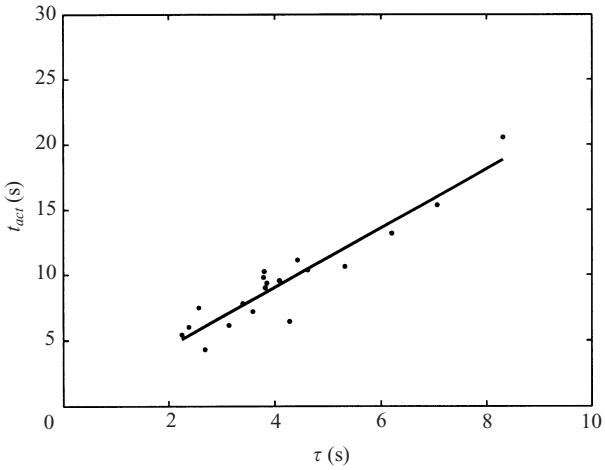



FIGURE 7. The actual time of arrival of the LEE ($t_{act}$) for all experiments as a function of the time scale $\tau$, defined in the text.

and so the time scale for the time of arrival at position $y$ is given by

$$\tau \sim \left( \frac{y\sqrt{Pr}}{g\beta\Delta T} \right)^{1/2}. \tag{6.3}$$

Figure 7 shows the observed arrival times of the leading-edge effect plotted as a function of $\tau$. It is immediately clear that although there is some scatter, the arrival times are approximately a linear function of $\tau$, and a linear regression through the data gives a slope of 2.27 with $R^2 = 0.88$. This supports the view that the leading-edge effect travels at a speed related to the speed of the travelling waves on the boundary layer.

## 7. Conclusions

The times determined from the experiments for the arrival of the leading-edge effect have been shown to be predicted well by the times evaluated from an integration of the maximum phase velocity of the waves generated at the leading edge at start-up. These results lend support to the model of Armfield & Patterson (1992) of the deviation from the purely one-dimensional solution into the transition flow occurring at the time given by the passage of the fastest travelling wave originating at the leading edge. Further, there is support for the view that the oscillatory component of the transition region is primarily the maximally amplified wavenumbers.

These conclusions do not address the actual mechanism which triggers the transition from the one- to two-dimensional solution, or discuss the role that the pressure signal, which must be present, plays in the transition. Indeed, numerical solutions of the cavity problem indicate that deviation on very small scales occurs at all positions along the boundary layer immediately after start-up. These are easily distinguishable from the arrival of the leading-edge effect which causes a deviation on a much larger scale. These are more difficult issues to deal with, and are beyond the scope of this paper.

The remaining issue is that of the alternative mechanism for the transition to two-dimensionality. Joshi & Gebhart (1987) observed it for the isoflux experiment, and the present results also clearly show a similar transition. Brooker *et al.* (2000) identified

https://doi.org/10.1017/S0022112001006553 Published online by Cambridge University Press

it with an instability associated with the input of perturbations to the boundary conditions present in the experimental rig, and suggested that this could occur at downstream locations prior to the arrival of the leading-edge effect. An analysis of this effect is outside the scope of the present paper, which focuses on the leading edge effect. However, we speculate that a further stability analysis of the unsteady boundary layer, seeking modes with temporal rather than spatial amplification, may reveal that some downstream region will become unstable prior to the arrival of the leading-edge effect. In these regions, it is possible that the transition to two-dimensional flow will occur by this alternative mechanism.

The experiments described here were carried out while T. G. was a student in the Department of Environmental Engineering at the University of Western Australia. W. S. was supported by a James Cook University postdoctoral fellowship. The research was supported by the Australian Research Council. This support is gratefully acknowledged.

## REFERENCES

Abramowitz, M. & Stegun, I. A. 1965 *Handbook of Mathematical Functions*. Dover.

Armfield, S. W. & Patterson, J. C. 1992 Wave properties of natural convection boundary layers. *J. Fluid Mech.* **239**, 195–211.

Brooker, A. M. H., Patterson, J. C. & Armfield, S. W. 1997 Non-parallel stability analysis of the vertical boundary layer in a differentially heated cavity. *J. Fluid Mech.* **352**, 265–281.

Brooker, A. M. H., Patterson, J. C., Graham, T. & Schöpf, W. 2000 Convective instability in a time dependent buoyancy driven boundary layer. *Intl J. Heat Mass Transfer* **43**, 297–310.

Brown, S. N. & Riley, N. 1973 Flow past a suddenly heated vertical plate. *J. Fluid Mech.* **59**, 225–237.

Daniels, P. G. & Patterson, J. C. 1997 On the long-wave instability of natural convection boundary layers. *J. Fluid Mech.* **335**, 57–73.

Gebhart, B., Jaluria, Y., Mahajan, R. L. & Sammakia, B. 1988 *Buoyancy Induced Flow and Transport*. Hemisphere.

Gebhart, B. & Mahajan, R. L. 1982 Instability and transition in buoyancy induced flows. *Adv. Appl. Mech.* **22**, 231–315.

Goldstein, R. J. & Briggs, D. G. 1964 Transient free convection about vertical plates and circular cylinders. *Trans. ASME: J. Heat Transfer* **86**, 490–500.

Jeevaraj, C. G. & Patterson, J. C. 1992 Experimental study of transient natural convection of glycerol-water mixtures in a side heated cavity. *Intl J. Heat Mass Transfer* **35**, 1573–1587.

Joshi, Y. & Gebhart, B. 1987 Transition of vertical natural convection flows in water. *J. Fluid Mech.* **179**, 407–438.

Ostrach, S. 1964 Laminar flows with body forces. In *Theory of Laminar Flows* (ed F. K. Moore), pp. 528–718. Princeton University Press.

Patterson, J. C. & Armfield, S. W. 1990 Transient features of natural convection in a cavity. *J. Fluid Mech.* **219**, 469–497.

Patterson, J. C. & Imberger, J. 1980 Unsteady natural convection in a cavity. *J. Fluid Mech.* **100**, 65–86.

Schetz, J. A. & Eichhorn, R. 1962 Unsteady natural convection in the vicinity of a doubly infinite vertical plate. *Trans. ASME: J. Heat Transfer* **84**, 334–338.

Schladow, S. G. 1990 Oscillatory motion in a side heated cavity. *J. Fluid Mech.* **213**, 589–610.

Schöpf, W. & Patterson, J. C. 1995 Natural convection in a side heated cavity: visualization of the initial flow features. *J. Fluid Mech.* **295**, 357–379.

Schöpf, W. & Patterson, J. C. 1996 Visualisation of natural convection in a side-heated cavity: transition to the final steady state. *Intl J. Heat Mass Transfer* **39**, 3497–3510.

Siegel, R. 1958 Transient free convection from a vertical flat plate. *Trans. ASME: J. Heat Transfer* **80**, 347–359.

Wright, N. T. & Gebhart, B. 1994 The entrainment flow adjacent to an isothermal vertical surface. *Intl J. Heat Mass Transfer* **37**, 213–231; 347–359.

https://doi.org/10.1017/S0022112001006553 Published online by Cambridge University Press